National Forest Biomass Mapping Using the Two-Level Model

Henrik J. Persson , *Senior Member, IEEE*, Maciej J. Soja, *Member, IEEE*,
Johan E. S. Fransson, *Senior Member, IEEE*, and Lars M. H. Ulander , *Fellow, IEEE*

Abstract—This article uses the two-level model (TLM) to predict above-ground biomass (AGB) from TanDEM-X synthetic aperture radar (SAR) data for Sweden. The SAR data were acquired between October 2015 and January 2016 and consisted of 420 scenes. The AGB was estimated from forest height and canopy density estimates obtained from TLM inversion with a power law model. The model parameters were estimated separately for each satellite scene. The prediction accuracy at stand-level was evaluated using field inventoried references from entire Sweden 2017, provided by a forestry company. AGB estimation performance varied throughout the country, with smaller errors in the north and larger in the south, but when the errors were expressed in relative terms, this pattern vanished. The error in terms of root mean square error (RMSE) was 45.6 and 27.2 t/ha at the plot- and stand-level, respectively, and the corresponding biases were −8.80 and 11.2 t/ha. When the random errors related to using sampled field references were removed, the RMSE decreased about 24% to 20.7 t/ha at the stand-level. Overall, the RMSE was of similar order to that obtained in a previous study (27–30 t/ha), where one linear regression model was used for all scenes in Sweden. It is concluded that, using the power law model with parameters estimated for each scene, the scene-wise variations decreased.

Index Terms—Forestry, interferometry, synthetic aperture radar (SAR), vegetation mapping.

I. INTRODUCTION

I N SWEDEN, remote sensing has long been used for wall-to-wall forest mapping, demanded both by the wood industry and for more general mapping of natural resources. In the past, satellite-based images with 25 m resolution were a valuable resource. More recently, the entire country was laser scanned, which resulted in forest mapping products [including forest height and above-ground biomass (AGB)] with 12.5 m resolution, with the majority of the forest covered between 2009 and 2015 [1]–[3]. However, due to the active management of

Swedish forests and strict requirements on forest data, these mapping products have already become outdated in many areas. There is, therefore, a widespread demand for new, accurate mapping products that can be repeated more frequently.

Since 2010, the German synthetic aperture radar (SAR) mission TanDEM-X has been mapping the Earth in order to generate a new, global, accurate digital elevation model [4]–[6] and provide spatial data for scientific use. It consists of two satellites flying in a close formation, enabling bistatic acquisitions with minimal temporal decorrelation. This X-band system (3.1 cm wavelength) has proven to be an accurate tool for mapping of forests [7]–[15], especially in areas with known topography, where the phase height (PH), i.e., the elevation of the scattering phase center above ground, can be determined. Many studies have demonstrated that PH and AGB (or the closely related stem volume) have a near-linear relationship [9], [11], [16], [17]. In [16], national biomass and stem volume rasters were generated for entire Sweden from the PH only, using one linear model for the entire country.

In [8], it was observed that PH showed different sensitivity to AGB in two test sites in Sweden, separated by almost 6° in latitude, indicating the dependence of PH on forest type and/or structure. Moreover, the exact relationship between PH and AGB also depends on system parameters, such as baseline, incidence angle, and polarization.

Numerous interferometric models and associated inversion techniques have been introduced in the past to explain the dependence of InSAR data on valuable forest parameters. The interferometric water cloud model (IWCM) was first introduced in [18]–[20] to explain the dependence of single-polarized, repeat-pass interferometric C-band ERS-1/2 coherence on stem volume, but it was later adapted for estimation of AGB from TanDEM-X data over areas with known topography [21]. The random volume over ground (RVoG) model was initially introduced in [22] and [23] to estimate forest height from fully polarimetric InSAR data, but was later extended for both forest height and biomass estimation from TanDEM-X data [12], [13]. The two-level model (TLM) was introduced in [7] as a simplified version of both IWCM and RVoG, allowing direct estimation of both forest height and canopy density from single-polarized InSAR data over boreal forests with known topography, without the need for additional data (allometric models in the case of IWCM, additional polarizations in the case of RVoG). In [8], the two forest properties obtained from TLM inversion in [7] were used for accurate AGB estimation over two test sites in Sweden,

TABLE I
AGB PROPERTIES FOR FIELD DATASETS

Dataset	Mean (t/ha)	Sd (t/ha)	Min (t/ha)	Max (t/ha)	N
NFI (all plots)	91.9	74.3	0	598.1	25 520
NFI (training plots)	106.6	64.9	15.0	505.2	22 284
Sveaskog (evaluation stands)	73.8	46.8	0	335.6	1 704

whereas in [24], TLM was used with multitemporal TanDEM-X data for monitoring of deforestation and forest growth.

In [25], stem volume prediction performance was assessed for a TanDEM-X scene in northern Sweden for two scenarios: direct estimation from PH using a regression model, and regression-based estimation using forest height and canopy density metrics obtained from TLM inversion [7], [8]. In both cases, local plot data from the Swedish National Forest Inventory (NFI) were used for estimating the regression model parameters. It was found that local estimation of model parameters improved the prediction performance compared with the approach where a single model was used for the entire country [16]. No significant difference could be found between the two scenarios.

In the previous studies, [16] and [25], a change of the relationship between PH and AGB was observed for satellite acquisitions made under frozen ground conditions. However, when model parameters are estimated individually for each scene, rather than nationally, such limitations can potentially be overcome. In addition, this approach enables additional analyses, such as influence of geographic location (i.e., latitude and longitude) and weather conditions (primarily temperature and precipitation).

The objectives of this article are first, demonstrating a large-scale application of the TLM for more accurate predictions of AGB. Second, evaluating the large-scale AGB estimation performance at stand-level, with respect to geographic location and weather conditions. Finally, using an error model to describe how the performance changes with reference AGB.

II. MATERIAL AND METHODS

A. Study Area

Sweden was used as study area for this article. The country has a land area of 41 million ha, of which 24 million ha is productive forest. Sweden is located mainly in the boreal forest region, although the southernmost parts are within the hemi-boreal and nemoral regions. About 5.0 million ha cover mountainous vegetation, 5.1 million ha are wetland, and 2.8 million ha are farming land [26]. The forest is dominated by Norway spruce (*Picea abies* (L.) H. Karst), Scots pine (*Pinus sylvestris* L.), and birch (*Betula* spp.), where pine and spruce constitute about 80% of the growing stock and birch about 12%. The current total AGB is more than 1 800 million tonnes, with an average AGB of 1 800 tonnes per hectare (t/ha). The forest can locally reach approximately 600 t/ha (Table I), according to the Swedish NFI.

B. Field Data

Two datasets with field references were used. First, plot-level data from the Swedish NFI were used to estimate the model
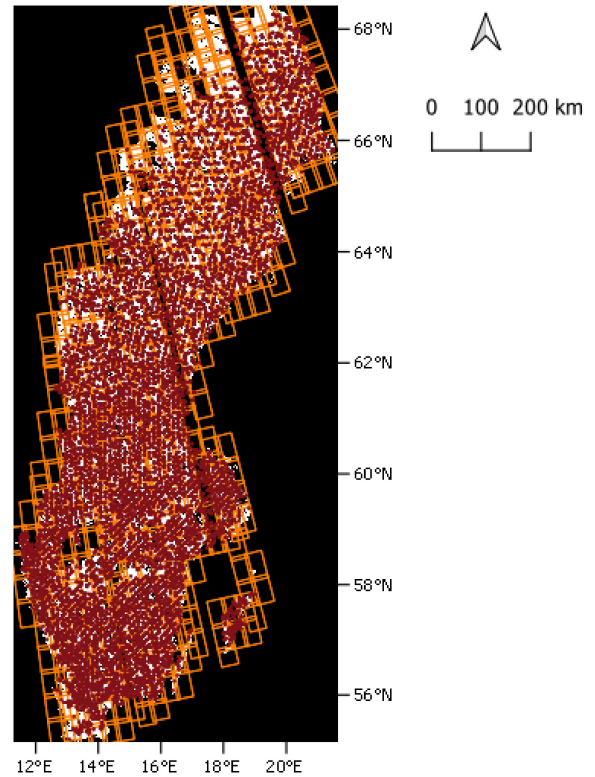

Fig. 1. Coverage of Sweden with the NFI plots (red) used for estimation of model parameters. The TanDEM-X scenes are outlined in orange.

parameters (training) with regression. The NFI inventories annually about 11 000 permanent (10 m radius) and temporary (7 m radius) field plots, randomly located all over Sweden [27], [28]. The plots are located in clusters, with separations of several hundreds of meters to ensure no spatial autocorrelation. The distances vary over the country, with larger separations further north. For this article, only forested plots were selected (Fig. 1), and the reference AGB was computed using established equations [29], [30] using trees with a diameter at breast height (DBH) $\geq$ 4 cm. To obtain a sufficient number of plots for each satellite scene (20 were selected as lower limit), field data from the entire period of 2007 to 2016 were used, and growth until 2016 was predicted for plots with outdated estimates [31]. This resulted in on average 72 available plots per satellite scene, and in total 25 520 unique plots for the entire country, where 333 scenes fulfilled the criteria of at least 20 plots. This was enough to cover all forest in Sweden, since most scenes that were excluded were located along the coastal borders with large parts located in the sea, or along the mountain ridge, which has no forest. The AGB properties of the field dataset are presented in Table I.

The second field dataset was provided by Sveaskog, a state-governed Swedish forestry company. In 2017, they carried out an extensive field inventory of 2 400 forest stands, distributed all over Sweden. The purpose was to obtain an accurate estimate of their entire forest holding, reference data for prediction modeling, and evaluation data for their previous forest management. Due to the time difference between the satellite and field datasets, clear-cut stands, and also stands largely overlapping with nonforest land features (e.g., roads and mires), were removed.

TABLE II
STAND SIZE PROPERTIES FOR FIELD EVALUATION DATASET

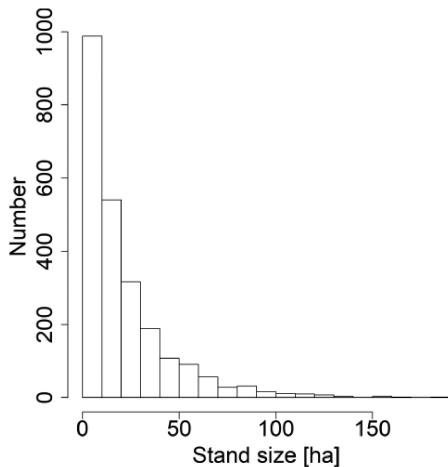| Dataset	Mean (ha)	Sd (ha)	Min (ha)	Max (ha)	N
Sveaskog (evaluation stands)	21.2	23.2	0.360	186.9	1 704

Fig. 2.   Distribution of stand size in hectare for the stands used for evaluation.

This resulted in a total of 1 704 forest stands used for the evaluation (Tables I and II). The inventoried stands were sampled with circular plots of dynamic radius (from 5 to 10 m), using a probability sample approach with a systematic grid, but with random reference location. The radius was fixed for all plots within a stand, but adjusted between stands, to obtain on average 15 to 20 trees per plot. This approach led to an average of 7 plots per stand (5 to 12, depending on the stand size and shape). The separate plot averages were used to compute the variance at stand-level. Trees with a DBH > 4 cm were measured and the species registered. The plot-level AGB was computed using the same approach as for the NFI plots in the first dataset. Stand-level estimates were computed as plot averages for each stand, and the dominant tree species was determined. The stand size properties are presented in Table II, and the distribution of stand size is presented in Fig. 2.

In addition to field data, meteorological data in terms of air temperature and precipitation were acquired from the closest station available from the Swedish Meteorological and Hydrological Institute (SMHI). SMHI provided a network of 226 weather stations, distributed across Sweden. For each scene, the station with the shortest distance from the scene center was selected, and the average daily temperature and the average daily precipitation were obtained for the dates before each acquisition, as the average values for the 1, 3, 7, and 14 preceding days.

C. Remote Sensing Data

This study used 420 TanDEM-X acquisitions collected over Sweden between October 2, 2015, and January 31, 2016. The height-of-ambiguity (HOA) is a crucial parameter determining the sensitivity of InSAR data to forest height [23], [32], [33]. For all used images, the HOA was between 46 and 68 m, resulting in good forest height sensitivity and low likelihood of phase ambiguities. The corresponding range of the effective baselines was 107 to 139 m. The images were acquired during late fall and winter conditions, with temperatures ranging from $-32°C$ to $+11°C$. The images were acquired in strip-map mode, HH polarization, and with the single-look complex resolution of 2.5 m in slant range and 3.3 m in azimuth. The incidence angles at the scene centres were all between 38° and 45°.

A digital terrain model (DTM) derived from the national laser scanning data was provided by Lantmäteriet (the Swedish National Land Survey) at 2 m resolution and with a height accuracy better than 0.5 m. The DTM was used as ground reference during interferometric processing.

D. SAR Processing

The TanDEM-X data were delivered in the Coregistered Single look Slant range Complex format. Following a rather common processing approach, explained extensively in [16], a complex interferogram ($\tilde{\gamma}$) was computed using

$$\tilde{\gamma} = \frac{\langle s_1 s_2^* e^{-i\phi_0} \rangle}{\sqrt{\langle |s_1|^2 \rangle \langle |s_2|^2 \rangle}} \tag{1}$$

where s_1 and s_2 are the two interferometric images, $*$ is the complex conjugate operator, ϕ_0 is the interferometric phase due to topographic variations, and $\langle \cdot \rangle$ denotes spatial averaging using a window of 5×5 in range and azimuth, respectively.

Generally, the estimated value of $\tilde{\gamma}$ contains up to four different contributions: spatial decorrelation due to geometric differences between s_1 and s_2, temporal decorrelation due to changes occurring between the two acquisition dates, system decorrelation due to system and processing artefacts, and signal-to-noise decorrelation due to different noise representations. However, for a well-designed, bistatic system like TanDEM-X, with suitable preprocessing (including common band- and wavenumber shift-filtering), and a large number of averaged samples in (1), $\tilde{\gamma}$ can be assumed to be dominated by volume decorrelation, caused by the vertical distribution of scattering targets within the imaged scene, with good forest mapping results [7], [8].

E. Two-Level Model

Volume decorrelation can be modeled for a given backscattering profile $\sigma(z)$ as [18], [19]

$$\tilde{\gamma}_{\text{vol}} = \frac{\int_{-\infty}^{\infty} \sigma(z) e^{ik_z z} dz}{\int_{-\infty}^{\infty} \sigma(z) dz} \tag{2}$$

with z being the height above ground and k_z being the vertical wavenumber, which for a bistatic acquisition geometry is

$$k_z = \frac{2\pi}{\text{HOA}} = \frac{2\pi B_\perp}{\lambda R \sin\theta} \tag{3}$$

where HOA is the height-of-ambiguity, $B_\perp$ is the perpendicular baseline, λ is the wavelength, R is the average range, and θ is the local angle of incidence. HOA is the height corresponding to a 2π-phase shift in the interferogram, and it is the maximal

height difference, which can be unambiguously resolved by the interferometric system.

In the TLM, see [7], [8], [16], and [24], the forest is modeled as two discrete scattering levels, ground and vegetation, separated by the distance h. The vertical backscattering profile $\sigma(z)$ can thus be described as

$$\sigma\ (z) = (1 - \eta)\ \sigma^0_{gr}\delta\ (z) + \eta\sigma^0_{veg}\delta\ (z - h) \qquad (4)$$

where σ^0_{gr} is the backscattering coefficient at the ground level, σ^0_{veg} is the backscattering coefficient for the vegetation, η is the area-fill factor (the fraction of the total area covered by the vegetation level), and $\delta(\cdot)$ is the Dirac delta function. When inserted in (2) and integrated, the expression simplifies to

$$\tilde{\gamma}_{\mathrm{TLM}} =\ 1 - \zeta + \zeta e^{ik_z h} \qquad (5)$$

where ζ is the vegetation scattering fraction

$$\zeta\ =\ \frac{\eta}{\rho + \eta\,(1 - \rho)} \qquad (6)$$

and $\rho\ =\ \sigma^0_{gr}\,/\sigma^0_{veg}$ is the ground-to-vegetation backscatter ratio (when set to 1, equal ground and vegetation backscattering coefficients are assumed).

If volume decorrelation is the dominant contribution to $\tilde{\gamma}$, h, and ζ can be estimated from $\tilde{\gamma}$ by letting $\tilde{\gamma} = \tilde{\gamma}_{\mathrm{TLM}}$, e.g., using the equations provided in [7], [8]. The estimated h and ζ can then be used as AGB predictors in a power law model, further described in [8]

$$\mathrm{AGB}\ =\ K h^{\alpha}\zeta^{\beta} \qquad (7)$$

where K, α, and β are model parameters to be estimated from reference data (in the following, NFI plots within each scene were used as reference). As discussed in [8], the model (7) can be motivated using a geometric argument, and it is similar to empirical models used in laser scanning-based AGB estimation, where h and ζ are typically replaced by a suitable height percentile and canopy density or canopy cover metric [9], [34].

F. Parameter Estimation

For each scene, the required SAR metrics were extracted as mean values of the 30 m radius surrounding the available NFI plot centers. This does not completely match the field plot radii (7 and 10 m), but previous studies ([16], [25]) have shown, that the use of a slightly larger area of the SAR data decreases the variability and improves the estimation accuracy, in terms of lower standard error. Twenty plots were used as lower limit to estimate the parameters, otherwise the scene was skipped. The PH values around 0 m can also cause instabilities due to wrapping problems. To automatically identify such plots, the average of the vegetation height of the pixels in the plot was compared with the vegetation height obtained after averaging the complex coherence over the plot followed by computing h and ζ. Plots where the difference exceeded 2 m were assumed noisy outliers and were hence removed. Additionally, plots with $h < 0$ were removed, since negative vegetation heights have no physical meaning, and they often appeared for plots with (almost) no forest. To filter out erroneous NFI plots (primarily due to clear-cuts after the inventory), regression was used and the
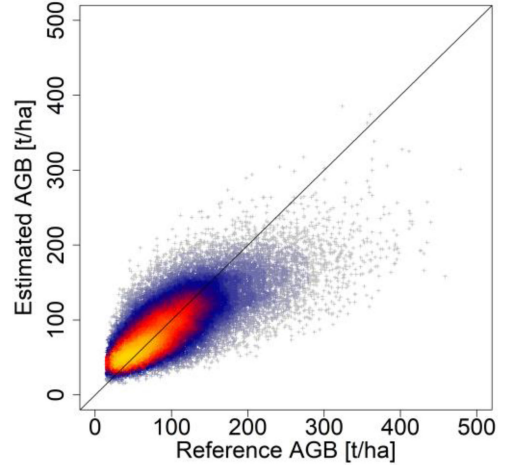

Fig. 3. Scatter plot of AGB estimated with TLM versus field reference plots.

estimated plots with $|\mathrm{residuals}| > 2.5$ standard deviations were removed. Then, (7) was linearized using the natural logarithm, and linear regression was used to estimate the parameters K, α, and β. The estimated model was used to predict the AGB for all pixels within the current scene. Since the TanDEM-X scenes were overlapping, some of the NFI plots were used several times, for different scenes. When "double counting" NFI plots, 31 526 were available and 22 284 plots used for estimating the model parameters (compared with 25 520 in Table I). The scatter plot (Fig. 3) illustrates the estimated versus reference AGB at plot-level (training data). In total, 333 scenes passed the processing criteria, which was still sufficient to cover the Swedish forest, since the removed scenes were located along the coasts (with a large fraction of the scene coverage over the sea), in the mountains above the tree line, or over larger cities (Fig. 4). However, two satellite passes did not fulfil the HOA selection criteria and these areas are shown as missing data in Fig. 4.

G. Evaluation

The AGB model (7) was evaluated with the NFI plots and stand level inventory data, using root mean square error (RMSE) and bias defined as

$$\mathrm{RMSE} = \sqrt{\frac{1}{n}\sum_{i=1}^{n}\left(\widehat{Y}_i - Y_i\right)^2} \qquad (8)$$

$$\mathrm{Bias} = \frac{1}{n}\sum_{i=1}^{n}\left(\widehat{Y}_i - Y_i\right) \qquad (9)$$

with Y being the reference, and $\hat{Y}$ the prediction for plot or stand i, and n denoting the number of plots or stands.

Additionally, the predicted error at stand-level was estimated with a linear error model [35], which enabled comparisons with other studies using other datasets, and it also enabled a graphical illustration of how the error changed with the reference value. The error model was defined as in [35]

$$T_{\mathrm{RS}} = \lambda_0\ + \lambda_1 \cdot T + \varepsilon \qquad (10)$$
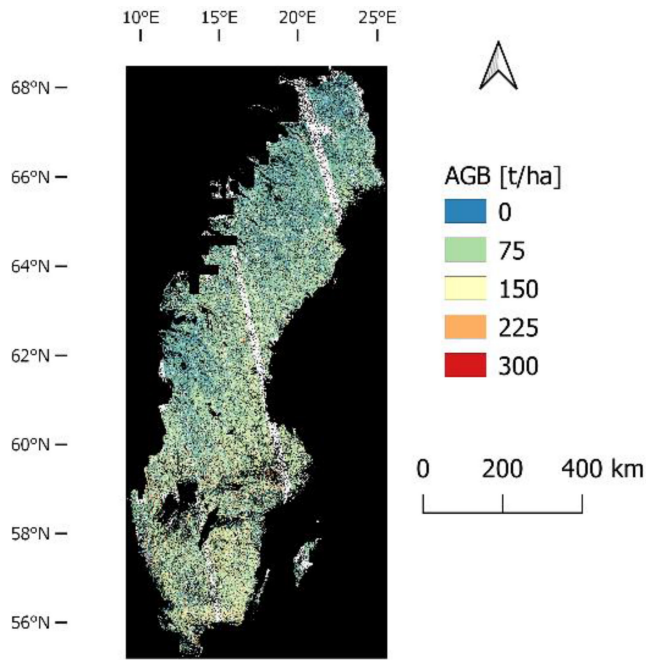
Fig. 4. Swedish prediction map of forest AGB, mosaicked from 333 TanDEM-X satellite scenes. The white stripes represent missing data.

TABLE III
RESULTS OF TRAINING (PLOTS) AND EVALUATION (STANDS)

Dataset	Variable	RMSE (t/ha)	Bias (t/ha)
Training	AGB	45.6 (42.8%)	-8.80 (-8.25%)
Evaluation	AGB	27.2 (36.8%)	11.2 (15.2%)

where T_{RS} denotes the RS-based estimate, T is the true AGB value, λ_0 is a systematic displacement, λ_1 makes the systematic error change across the range of true values, and ε denotes the random errors. There were two main purposes for using the error model. First, to illustrate how the error varies with varying reference value, instead of reporting a single value as RMSE. Second, the error model provides estimates of the errors in the field data, which were propagated to the reported ordinary RMSE. It, therefore, allowed to also report the corrected ($*$) RMSE*, where the variance contribution due to random errors in the field data was removed (which was assumed to appear due to the use of a sample instead of a completely inventoried reference). Sampling errors are known to dominate the random errors in field estimates [36].

III. RESULTS

A Training and Evaluation of Models

The models were validated on the NFI plots used as training data, and evaluated on the stand-level inventory data provided by Sveaskog.

The prediction error of AGB in terms of RMSE was larger for the training data (45.6 t/ha) than the evaluation data (27.2 t/ha), see Table III. This can be explained with the training data representing plots of a few hundred m², while the evaluation
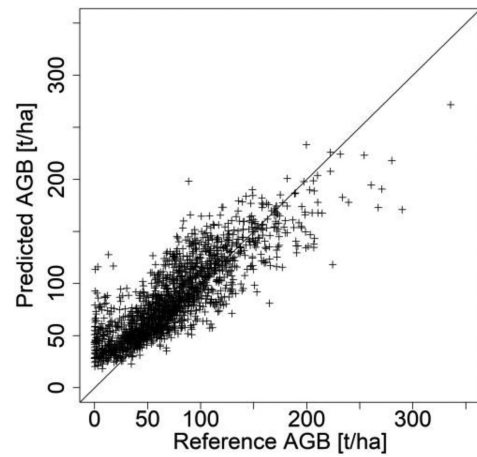

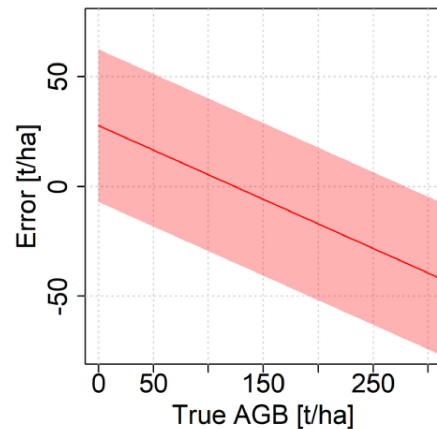Fig. 5. Scatter plot of AGB predicted with TLM versus field reference at stand-level.

Fig. 6. Visualization of the error structure for the stand-level evaluation. The solid line is due to the residuals, computed from λ_0^* and λ_1^*, and the band width represents the random errors as $\pm 2\sigma_\varepsilon^*$.

TABLE IV
ERROR MODEL RESULTS

Parameter	Value
λ_0^*	27.7
λ_1^*	0.776
σ_ε^{2*}	302
RMSE* (t/ha)	20.7 (28.0%)
Bias* (t/ha)	11.2 (15.2%)

stands could be much larger (Table II). The bias for the training was negative (-8.80 t/ha), while the evaluated stands had a positive bias (11.2 t/ha), see Table III. In the predicted versus reference scatter plot (Fig. 5), some plots with low reference AGB suffer from biomass overestimation. This can also be observed in Fig. 6, which is a graphical illustration of the error model (10) with parameters presented in Table IV. The residuals were positive for low reference values, but then they were decreasing until a negative bias was obtained for the largest reference values.

TABLE V
ESTIMATED PARAMETERS

Parameter	Median	Mean	Min	Max	Sd
K	42.0	108	0.263	1014	162
α	0.596	0.639	-0.738	2.77	0.605
β	0.931	0.963	0.125	1.77	0.269

The variance (due to random errors) was substantial, which could be seen in the parameter σ_ε^{2*} in Table IV. Therefore, it exceeded the bias (11.2 t/ha corresponds to 125 t^2/ha^2) as the largest contributor to the MSE, although both error contributions were of similar order. When the random errors (in terms of sampling errors) were accounted for in the field data, the RMSE decreased to 20.7 t/ha (28.0%). This implied, that approximately 23.9% of the original RMSE for evaluation (27.2 t/ha, Table III) was due to sampling errors in this dataset.

B. Parameters

The parameters K, α, and β (estimated from the training dataset) varied from scene to scene (Table V), where the scaling factor K was fluctuating the most, and generally being larger than in previous studies (these indicated K between 0 and 30, α between 1 and 2, and β between 1 and 3) [25], [37]. A larger value of K was compensating for a decreased sensitivity in h and ζ, possibly due to the data being acquired in colder (and leaf-off) conditions (as opposed to [8], where only summer acquisitions were used). This was partly due to α being mostly between 0 and 1, which was related to the vegetation height h that tends to be lower during colder conditions. The parameter β was related to the canopy density ζ, which appeared to be less affected by changing weather conditions. It was also most similar to previous results.

Some of the predicted scenes passed the modeling criteria in Section II, but with very large estimations of the K parameter. These scenes were mostly estimated with a negative α, which appeared when the AGB approached zero, and caused an increase of K. The correlation between K and α was -0.70, and the corresponding correlation of K and β was 0.078. The scenes with extraordinary K and α values were covering areas with low biomass, and with PHs of only a couple of meters. These observations confirm past experiences [7], [8], [38], [39], which have shown that in this range of PHs, decorrelation effects other than volume decorrelation are erroneously interpreted as volume decorrelation, yielding significant forest height overestimation, which then is compensated for with low α-values and high K-values.

C. Influence of Location and Weather

The influence of location and weather conditions on the parameter values was investigated for the training dataset (plot-level). There were generally no strong tendencies concerning location (Fig. 7), which indicated that the method is rather robust against different latitudes and longitudes.

Neither could any clear trends be noticed when the parameters were plotted against temperature and precipitation (Fig. 8). This
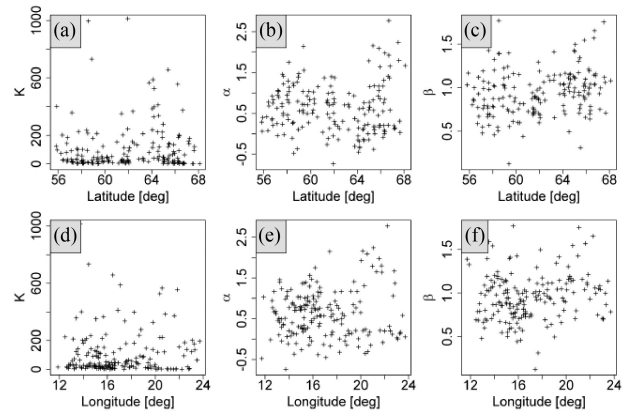

Fig. 7. Scatter plots of parameters versus latitude (a–c) and longitude (d–f).
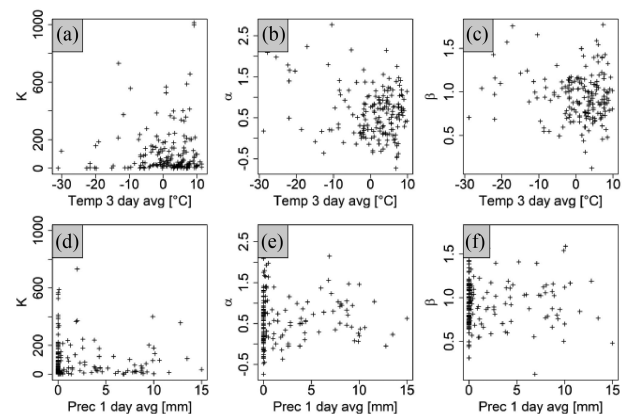

Fig. 8. Scatter plots of parameters versus 3-day average temperature (a–c) and parameters versus 1-day average precipitation (d–f).

increases the potential of using the TLM approach in various weather conditions. Although there was not a clear trend with varying temperature in these data (regardless of temperature length, 1 to 14 days), it has been reported that the freezing of trees affects the PH by reducing the dielectric constant [16], [40]–[42]. To capture this effect, a 1-day average was assumed too short to thaw frozen trees, while a too long sequence was expected to disguise the changes actually appearing due to freezing. Therefore, the scatter plots in Fig. 8 are showing the 3-days average of temperature, and 1-day average of precipitation. The precipitation was expected to affect the scattering directly, as long as the forest was wet, and after three or more days such water has usually evaporated.

The influence of location and weather conditions with respect to the error, expressed as RMSE, was also investigated for the training dataset. At first, a strong trend between the RMSE and the location could be observed, both for latitude and longitude (Fig. 9). However, since the AGB and height were generally higher further south and closer to the coasts, plotting of the relative RMSE eliminated this trend entirely.

A similar relation was noticed for temperature (Fig. 10), where the temperatures were generally higher further south and closer to the coasts. Hence, by observing the relative RMSE,
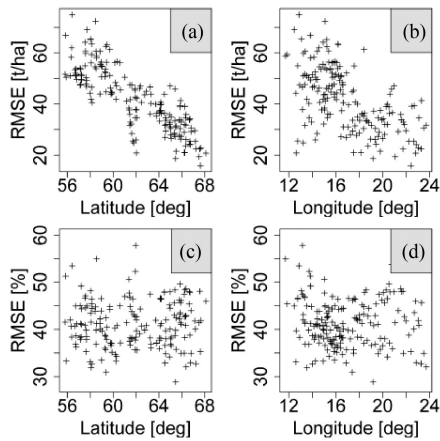
Fig. 9. Scatter plots of RMSE versus latitude and longitude in absolute terms (a and b) and relative (%), (c and d).

Fig. 11. Scatter plot of predicted AGB versus reference divided per dominant tree species.
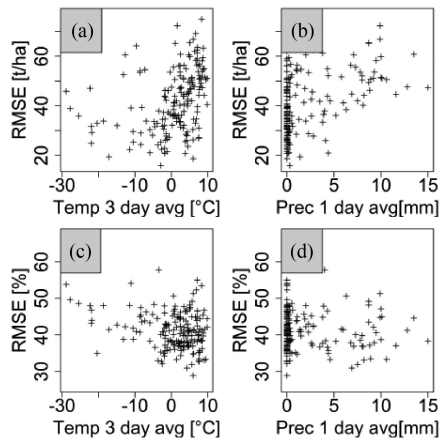

Fig. 10. Scatter plots of RMSE versus 3-day average temperature and 1-day average precipitation (a and b) and RMSE in % (c and d).

the weather-induced effects were eliminated. Furthermore, no precipitation appeared to have any clear impact on the relative RMSE.

D. Influence of Tree Species

For the evaluation dataset, the dominant tree species was registered for each forest stand. Therefore, the predicted versus reference AGB could be plotted (Fig. 11) for the major tree species (pine, spruce, and birch), which constitute more than 90% of the AGB at the national level. The influence of different tree species was found negligible, with almost no differences other than that spruce forest were generally reaching the highest AGB, and the AGB at these levels were often underestimated.

IV. DISCUSSION

The TLM has been tested extensively in the past, especially at the two Swedish test sites Remningstorp and Krycklan [7], [8], [24], [37], but this article showed a promising performance for many more scenes, covering a large area, and acquired during more uncertain conditions with regard to weather aspects. The
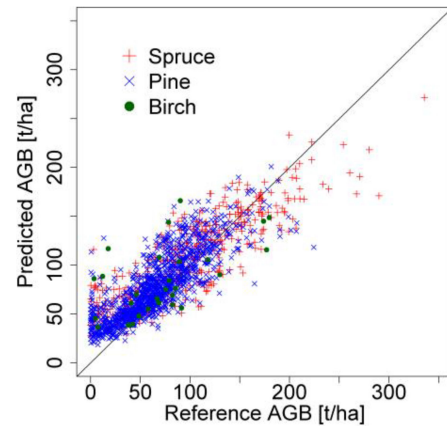
evaluated approach appeared robust in a variety of weather conditions and for various forest types, despite a large observed range of model parameters. The accuracy in terms of RMSE (27.2 t/ha, Table III) was similar as in a previous study (27.4 to 29.7 t/ha) that used the same TanDEM-X dataset, but slightly different reference data [16]. The bias was also at approximately the same levels (-8.80 to 11.2 t/ha for plot- and stand-level, compared to -6.17 to 10.5 t/ha for two stand-level datasets) [16].

The approach of estimating the parameters individually for each scene reduced the border effects between neighboring scenes, which was caused by large scene-to-scene variations and observed in a previous large-scale study [16]. This facilitates mosaicking, but it also requires a rather extensive reference dataset. Since the preprocessing of the TanDEM-X data also requires a DTM, the presented approach might be most suitable for frequent, large-scale mapping of forests for applications such as commercial forestry and disaster management when an accurate DTM is available.

A. Estimation Accuracy

A clear biomass overestimation was observed for forests with low AGB (< 50 t/ha), most often represented by young or sparse forest, with a lower tree height. This type of forest typically has a larger ground contribution to the scattered radar signal than a taller and denser forest, thus affecting the relation between ζ and AGB. As the power law model parameters were estimated individually for each scene using NFI plots, their values are most optimal for forest types well-represented within the training data. Moreover, for forests with lower heights, volume decorrelation becomes less significant in comparison with other decorrelation effects (mainly system and SNR decorrelation), and the assumption of $\tilde{\gamma} = \tilde{\gamma}_{TLM}$ is no longer valid. However, if the assumption is still used, other decorrelation effects are interpreted as volume decorrelation, leading to inflated forest height estimates, as discussed in [7] and [8]. These effects result not only in the observed AGB-dependent bias, but also in the large observed variability of the power law model parameters across the scenes.

Two potential approaches can be used to mitigate the observed AGB-dependent biases. First, prestratification of the forest type can be used to estimate the parameters to the particular forest structure, albeit at the cost of increased complexity of model parameter estimation. Second, this issue can be decreased using multitemporal and multibaseline data and additional approaches correcting for decorrelation effects other than volume decorrelation and changing values of the ground-to-vegetation backscatter ratio (ρ), as proposed in [24].

The negative bias observed for the training data may appear unexpected, since regression was used to estimate the parameters, but since linear regression was used with model (7) transformed into the logarithmic domain, there was a nonlinear relation of the bias when it was transformed back into linear units. A correction for this logarithmic bias was tested but found unsuccessful [43].

B. Error Model Implications

The stand-level accuracy (37% RMSE) is reasonably good for Swedish conditions at the national level, although airborne laser scanning (ALS)-based approaches give a better accuracy with correspondingly about 17% to 22% [3]. However, comparisons with other studies using relative accuracies may be misleading, since it greatly depends on the mean of the sampled distribution.

Field-based methods using a relascope can often provide stand-wise estimations of AGB and stem volume with about 15% RMSE, whereas systematic sampling using objectively distributed circular plots can be in the range of 12% to 20% RMSE, depending on the number of plots and the homogeneity of the stand (normally about 4 to 10 plots per stand) [44]. With a large number of plots, even more accurate estimates with smaller errors can be obtained with these methods (4% to 8%) [45], [46]. Such accuracy levels are better than the tested TanDEM-X approach, but field samples are also restricted to much smaller regions and requires substantially more work, making them poorly suited for frequent forest mapping.

By applying the error model approach, the understanding for the error was improved. From Fig. 6 it could be seen that the lowest error was obtained for AGB values between 100 and 150 t/ha, and from Table IV it was noted that the variance ($\sigma_{\varepsilon}^{2*}$) was a larger source of error than the bias, when computing the RMSE. The error model provided estimators for compensation of the field induced errors, which in our case was assumed only due to the sampling approach. However, this error source was surprisingly large, and when this contribution was considered and adjusted for, the RMSE* decreased to 20.7 t/ha (28.0%). This means, that adjusting for the field induced sampling error removed 24% of the reported error. The error parameter values should be compared with other studies in the future, to better value the outcome of this article.

C. Influence of Location, Weather Conditions, and Forest Type

The large observed range of model parameters could not be explained with the scene location (Fig. 7) or weather conditions (temperature and precipitation, Fig. 8). Yet, these parameters should not be disqualified as possible reasons, since other larger disturbing factors may conceal a relation, especially when temperature and precipitation are considered. Many studies have indicated that weather factors affect SAR observations of forest [16], [40]–[42], [47].

The sampling intensity of reference plots provided by the NFI is sparser further north and closer to the mountains, which might have caused the use of a larger fraction of forecasted reference plots than in southern regions. The forecasting models are generally rather accurate [31], [48], but sudden changes, e.g., due to storms cannot be captured, and this may have induced noise that increased the instability of the parameter estimations.

The accuracy was similar regardless of the dominant tree species (Fig. 11), which indicated that there is not necessarily problems with mapping of deciduous forest during leaf-off conditions in the Scandinavian winter, at least not as long as all images are acquired within the same season. This should, however, be evaluated more extensively in future studies.

D. Relation to Other Models

A common and straightforward approach of applying InSAR data is the linear scaling of PH to AGB. This approach has shown good performance despite its simplicity, but it ignores the effect of the interferometric configuration (e.g., HOA) and it also requires reference data to estimate correct model parameters [9], [11], [17], [49], [50]. This increases the need of correctly selecting suitable acquisitions, but this approach is available and intuitive for most users.

Other approaches, e.g., the IWCM and the RVoG model, have also shown good performance in this type of studies, although RVoG was rarely used for direct AGB estimation [12], [21], [38], [39], [51]–[53]. To take advantage of their strengths, polarimetric data would be required for RVoG-based approaches and allometric equations would be needed for IWCM-based approaches. Without the additional information, simplifying assumptions are necessary to obtain a model with a sufficiently low number of unknown parameters with regards to available observations.

V. Conclusion

This article proved the suitability of large-scale mapping of forest AGB, using TanDEM-X data. Furthermore, the TLM predictions were robust against both various forest types and the most common weather effects (varying temperature and precipitation as rain and snow) in Scandinavian conditions. These aspects were investigated for the parameters that were estimated scene-wise. The parameters K and α varied largely between different scenes, and had a strong interdependence, whereas β was more stable under the varying conditions.

The scene-wise parameter estimation reduced the apparent scene-to-scene jumps in the predicted values, which is an advantage for mosaicking over larger regions, and this is an important conclusion compared to the approach of applying a single model for the entire country, as used in a previous study [16]. The accuracy in terms of RMSE was similar for both approaches. The AGB estimation performance is indicative for stem volume estimation as well, as these two metrics are highly correlated in Sweden.

The use of a linear error model [35] allowed for handling of errors in the field data, induced by using a sampling scheme. This improved the accuracy in terms of RMSE with about 24%, which was reduced to 20.7 t/ha, a similar order as some large-scale ALS applications. The error model parameters were used to visualize the error versus reference values, which improved the understanding for how the predictions were relating to the truth, and better relate the systematic errors to the random errors.

REFERENCES

[1] H. Reese *et al.*, "Countrywide estimates of forest variables using satellite data and field data from the national forest inventory," *Ambio*, vol. 32, no. 8, pp. 542–548, 2003.

[2] E. Tomppo, H. Olsson, G. Ståhl, M. Nilsson, O. Hagner, and M. Katila, "Combining national forest inventory field plots and remote sensing data for forest databases," *Remote Sens. Environ.*, vol. 112, no. 5, pp. 1982–1999, 2008.

[3] M. Nilsson *et al.*, "A nationwide forest attribute map of Sweden derived using airborne laser scanning data and field data from the national forest inventory," *Remote Sens. Environ.*, vol. 194, pp. 447–454, 2017.

[4] A. Gruber, B. Wessel, M. Martone, and A. Roth, "The TanDEM-X DEM Mosaicking: Fusion of multiple acquisitions using InSAR quality parameters," *IEEE J. Sel. Appl. Earth Observ. Remote Sens.*, vol. 9, no. 3, pp. 1047–1057, Mar. 2016.

[5] P. Rizzoli, B. Bräutigam, T. Kraus, M. Martone, and G. Krieger, "Relative height error analysis of TanDEM-X elevation data," *ISPRS J. Photogrammetry Remote Sens.*, vol. 73, pp. 30–38, Sep. 2012.

[6] C. Rossi *et al.*, "TanDEM-X calibrated Raw DEM generation," *ISPRS J. Photogrammetry Remote Sens.*, vol. 73, pp. 12–20, Sep. 2012.

[7] M. J. Soja, H. J. Persson, and L. M. H. Ulander, "Estimation of forest height and canopy density from a single InSAR correlation coefficient," *IEEE Geosci. Remote Sens. Lett.*, vol. 12, no. 3, pp. 646–650, Mar. 2015.

[8] M. J. Soja, H. J. Persson, and L. M. H. Ulander, "Estimation of forest biomass from two-level model inversion of single-pass InSAR data," *IEEE Trans. Geosci. Remote Sens.*, vol. 53, no. 9, pp. 5083–5099, Sep. 2015.

[9] H. J. Persson and J. E. S. Fransson, "Comparison between TanDEM-X and ALS based estimation of above ground biomass and tree height in boreal forests," *Scand. J. Forest Res.*, vol. 32, no. 4, pp. 306–319, 2017.

[10] M. J. Soja, J. I. H. Askne, and L. M. H. Ulander, "Estimation of boreal forest properties from TanDEM-X data using inversion of the interferometric water cloud model," *IEEE Geosci. Remote Sens. Lett.*, vol. 14, no. 7, pp. 997–1001, Jul. 2017.

[11] S. Solberg, R. Astrup, J. Breidenbach, B. Nilsen, and D. Weydahl, "Monitoring spruce volume and biomass with InSAR data from TanDEM-X," *Remote Sens. Environ.*, vol. 139, pp. 60–67, Dec. 2013.

[12] F. Kugler, D. Schulze, I. Hajnsek, H. Pretzsch, and K. P. Papathanassiou, "TanDEM-X Pol-InSAR performance for forest height estimation," *IEEE Trans. Geosci. Remote Sens.*, vol. 52, no. 10, pp. 6404–6422, Oct. 2014.

[13] A. Torano Caicoya, F. Kugler, I. Hajnsek, and K. P. Papathanassiou, "Large-scale biomass classification in boreal forests with TanDEM-X data," *IEEE Trans. Geosci. Remote Sens.*, vol. 54, no. 10, pp. 5935–5951, Oct. 2016.

[14] Y. Sadeghi, B. St-Onge, B. Leblon, and M. Simard, "Effects of TanDEM-X acquisition parameters on the accuracy of digital surface models of a boreal forest canopy," *Can. J. Remote Sens.*, vol. 43, pp. 1–14, 2017.

[15] H. Chen, A. Beaudoin, D. A. Hill, S. R. Cloude, R. S. Skakun, and M. Marchand, "Mapping forest height from TanDEM-X interferometric coherence data in northwest territories, Canada," *Can. J. Remote Sens.*, vol. 45, no. 3/4, pp. 290–307, 2019.

[16] H. J. Persson, H. Olsson, M. J. Soja, L. M. H. Ulander, and J. E. S. Fransson, "Experiences from large-scale forest mapping of Sweden using TanDEM-X data," *Remote Sens.*, vol. 9, no. 12, pp. 1253–1279, 2017.

[17] K. Karila, M. Vastaranta, M. Karjalainen, and S. Kaasalainen, "Tandem-X interferometry in the prediction of forest inventory attributes in managed boreal forests," *Remote Sens. Environ.*, vol. 159, pp. 259–268, 2015.

[18] J. O. Hagberg, L. M. H. Ulander, and J. Askne, "Repeat-pass SAR interferometry over forested terrain," *IEEE Trans. Geosci. Remote Sens.*, vol. 33, no. 2, pp. 331–340, Mar. 1995.

[19] J. I. H. Askne, P. B. G. Dammert, L. M. H. Ulander, and G. Smith, "C-band repeat-pass interferometric SAR observations of the forest," *IEEE Trans. Geosci. Remote Sens.*, vol. 35, no. 1, pp. 25–35, Jan. 1997.

[20] J. Askne, M. Santoro, G. Smith, and J. E. S. Fransson, "Multitemporal repeat-pass SAR interferometry of boreal forests," *IEEE Trans. Geosci. Remote Sens.*, vol. 41, no. 7, pp. 1540–1550, Jul. 2003.

[21] J. I. H. Askne, J. E. S. Fransson, M. Santoro, M. J. Soja, and L. M. H. Ulander, "Model-based biomass estimation of a hemi-boreal forest from multitemporal TanDEM-X acquisitions," *Remote Sens.*, vol. 5, no. 11, pp. 5574–5597, Oct. 2013.

[22] S. R. Cloude and K. P. Papathanassiou, "Polarimetric SAR interferometry," *IEEE Trans. Geosci. Remote Sens.*, vol. 36, no. 5, pp. 1551–1565, Sep. 1998.

[23] K. P. Papathanassiou and S. R. Cloude, "Single-baseline polarimetric SAR interferometry," *IEEE Trans. Geosci. Remote Sens.*, vol. 39, no. 11, pp. 2352–2363, Nov. 2001.

[24] M. J. Soja, H. J. Persson, and L. M. H. Ulander, "Modeling and detection of deforestation and forest growth in multitemporal TanDEM-X data," *IEEE J. Sel. Top. Appl. Earth Observ. Remote Sens.*, vol. 11, no. 10, pp. 3548–3563, Oct. 2018.

[25] H. J. Persson, M. J. Soja, J. E. S. Fransson, and L. M. H. Ulander, "Using the two-level model with TanDEM-X for large-scale forest mapping," in *Proc. IEEE Int. Geosci. Remote Sens. Symp.*, 2019, pp. 4484–4487.

[26] "Official statistical report from Swedish national forest inventory," Dept. Forest Resource Manage., Swedish Univ. Agricultural Sci., Skogsdata, Umeå, Sweden, 2019. [Online]. Available: https://www.slu.se/global assets/ew/org/centrb/rt/dokument/skogsdata/skogsdata_2019_webb.pdf

[27] J. Fridman, S. Holm, M. Nilsson, and P. Nilsson, "Adapting national forest inventories to changing requirements–the case of the Swedish National Forest Inventory at the turn of the 20th century," *Silva Fenn.*, vol. 48, no. 3, pp. 1–29, 2014.

[28] B. Ranneby, T. Cruse, B. Hägglund, H. Jonasson, and J. Swärd, "Designing a new national forest survey for Sweden," Swedish Univ. Agricultural Sci., Uppsala, Sweden, Tech. Rep., 1987.

[29] L. G. Marklund, "Biomass functions for pine, spruce and birch in Sweden," Dept. Forest Survey, Swedish Univ. Agricultural Sci., Umeå, Sweden, Rep. 45, 1988.

[30] G. Brandel, "Volume functions for individual trees; Scots pine (*Pinus sylvestris*), Norway spruce (*Picea abies*) and birch (*Betula pendula & Betula pubescens*)," Dept. Forest Survey, Swedish Univ. Agricultural Sci., Garpenberg, Sweden, Rep. 26, 1990.

[31] N. Fahlvik, B. Elfving, and P. Wikström, "Evaluation of growth functions used in the Swedish forest planning system Heureka," *Silva Fenn.*, vol. 48, no. 2, pp. 1–17, 2014.

[32] M. J. Soja and L. M. H. Ulander, "Digital canopy model estimation from TanDEM-X interferometry using high-resolution Lidar DEM," in *Proc. Int. Geosci. Remote Sens. Symp.*, 2013, pp. 165–168.

[33] G. Krieger and F. De Zan, "Relativistic effects in bistatic synthetic aperture radar," *IEEE Trans. Geosci. Remote Sens.*, vol. 52, no. 2, pp. 1480–1488, Feb. 2014.

[34] J. Holmgren, "Prediction of tree height, basal area and stem volume in forest stands using airborne laser scanning," *Scand. J. Forest Res.*, vol. 19, no. 6, pp. 543–553, 2004.

[35] H. J. Persson and G. Ståhl, "Characterizing uncertainty in forest remote sensing studies at plot and stand level," *Remote Sens.*, vol. 12, no. 3, pp. 1–21, 2020.

[36] G. Z. Gertner and M. Köhl, "An assessment of some nonsampling errors in a national survey using an error budget," *Forest Sci.*, vol. 38, no. 3, pp. 525–538, 1992.

[37] M. J. Soja, H. J. Persson, and L. M. H. Ulander, "Estimation of boreal forest biomass from two-level model inversion of interferometric TanDEM-X data," in *Proc IEEE Int. Geosci. Remote Sens. Symp.*, 2014, pp. 3398–3401.

[38] J. I. H. H. Askne, H. J. Persson, and L. M. H. Ulander, "Biomass growth from multi-temporal TanDEM-X interferometric synthetic aperture radar observations of a boreal forest site," *Remote Sens.*, vol. 10, no. 4, 2018, Art. no. 18.

[39] J. I. H. Askne, H. J. Persson, and L. M. H. Ulander, "On the sensitivity of TanDEM-X-observations to boreal forest structure," *Remote Sens.*, vol. 11, no. 14, pp. 1–22, 2019.

[40] C. Thiel and C. Schmullius, "Investigating the impact of freezing on the ALOS PALSAR InSAR phase over Siberian forests," *Remote Sens. Lett.*, vol. 4, no. 9, pp. 900–909, 2013.

[41] C. Thiel and C. Schmullius, "The potential of ALOS PALSAR backscatter and InSAR coherence for forest growing stock volume estimation in Central Siberia," *Remote Sens. Environ.*, vol. 173, pp. 258–273, 2016.

[42] R. Kwok, J. Holt, J. Way, and A. Freeman, "Polarization signatures of frozen and thawed forests of varying environmental state," *IEEE Trans. Geosci. Remote Sens.*, vol. 32, no. 2, pp. 371–381, Mar. 1994.

[43] D. M. Miller, "Reducing transformation bias in curve fitting," *Amer. Statistician*, vol. 38, no. 2, pp. 124–126, 1984.

[44] G. Ståhl, "A study on the quality of compartmentwise forest data acquired by subjective inventory methods," Umeå, Sweden, 1992.

[45] M. Piqué, B. Obon, S. Condés, and S. Saura, "Comparison of relascope and fixed-radius plots for the estimation of forest stand variables in northeast Spain: An inventory simulation approach," *Eur. J. Forest Res.*, vol. 130, no. 5, pp. 851–859, 2011.

[46] A. Karlsson, "Examination of inventory methods in final felling stands," (in Swedish), Dept. Forest Resource Manag., Swedish Univ. Agricultural Sci., Umeå, Sweden, Rep. 27, 1997.

[47] S. Solberg, D. J. Weydahl, and R. Astrup, "Temporal stability of X-band single-pass InSAR heights in a spruce forest: Effects of acquisition properties and season," *IEEE Trans. Geosci. Remote Sens.*, vol. 53, no. 3, pp. 1607–1614, Mar. 2015.

[48] K. Nyström and G. Ståhl, "Forecasting probability distributions of forest yield allowing for a Bayesian approach to management planning," *Silva Fenn.*, vol. 35, no. 2, pp. 185–201, 2001.

[49] Y. Sadeghi, B. St-Onge, B. Leblon, and M. Simard, "Canopy height model (CHM) derived from a TanDEM-X InSAR DSM and an airborne Lidar DTM in Boreal forest," *IEEE J. Sel. Top. Appl. Earth Observ. Remote Sens.*, vol. 9, no. 1, pp. 381–397, Jan. 2016.

[50] X. Yu *et al.*, "Comparison of laser and stereo optical, SAR and InSAR point clouds from air- and space-borne sources in the retrieval of forest inventory attributes," *Remote Sens.*, vol. 7, no. 12, pp. 15933–15954, 2015.

[51] A. T. Caicoya, F. Kugler, I. Hajnsek, and K. Papathanassiou, "Boreal forest biomass classification with TanDEM-X," in *Proc. Int. Geosci. Remote Sens. Symp.*, 2012, pp. 3439–3442.

[52] M. Lavalle and S. Hensley, "Extraction of structural and dynamic properties of forests from polarimetric-interferometric SAR data affected by temporal decorrelation," *IEEE Trans. Geosci. Remote Sens.*, vol. 53, no. 9, pp. 4752–4767, Sep. 2015.

[53] J. I. H. Askne, M. J. Soja, and L. M. H. Ulander, "Biomass estimation in a boreal forest from TanDEM-X data, lidar DTM, and the interferometric water cloud model," *Remote Sens. Environ.*, vol. 196, pp. 265–278, 2017.

Maciej J. Soja (Member, IEEE) was born in Warsaw, Poland, in 1985. He received the B.Sc. degree in engineering physics, in 2008, the M.Sc. degree in electrical engineering, in 2009, and the Ph.D. degree in radio and space science, in 2014, from the Chalmers University of Technology, Gothenburg, Sweden.

Between 2014 and 2017, he was a Postdoctoral Researcher and later Research Assistant in the Radar Remote Sensing Group with Chalmers University of Technology. Between 2017 and 2018, he worked as a Senior Research Officer for Horizon Geoscience Consulting Pty. Ltd., Belrose, NSW, Australia. Since 2018, he has been the Director and the Head Researcher of MJ Soja Consulting, Hobart, TAS, Australia. He also holds the position of Adjunct Researcher with the Discipline of Geography and Spatial Sciences, University of Tasmania, Hobart, TAS, Australia. Since 2009, he has been actively involved in the development of biomass estimation algorithm for the selected ESA P-band SAR mission BIOMASS. He has also participated in several EU and ESA projects, including Advanced SAR and GlobBiomass, and in the development of the tower radar experiment BorealScat. His main research interests include SAR mapping and monitoring of vegetation. His research experience also includes electromagnetic modeling and laser scanning data analysis.

Johan E. S. Fransson (Senior Member, IEEE) was born in Karlshamn, Sweden, in 1967. He received the M.Sc. degree in forestry and the Ph.D. degree in forest remote sensing from the Swedish University of Agricultural Sciences (SLU), Umeå, Sweden, in 1992 and 1999, respectively.

Since 1993, he has been with the Department of Forest Resource Management, SLU. In 2000 and 2002, he was employed as an Assistant Professor and appointed as an Associate Professor in forest remote sensing, respectively. He was the Head of Department 2008 to 2019 and is at present Deputy Head. He has authored or coauthored more than 200 professional publications, of which more than 40 are in peer-reviewed scientific journals. His main research interests include analysis of SAR images for forestry applications.

Dr. Fransson was the recipient of the International Space University Certificate from the Royal Institute of Technology in Stockholm, Sweden, in 1995, and the award from "Kungliga Skytteanska Samfundet" to a younger researcher at SLU, Umeå, in 2002. He has contributed to two paper awards (Forest Science and Remote Sensing).

Henrik J. Persson (Senior Member, IEEE) received the M.Sc. degree in engineering physics from Luleå Technical University, Luleå, Sweden, in 2009, and the Ph.D. degree in technology from the Swedish University of Agricultural Sciences (SLU), Umeå, Sweden, in 2014.

He is currently an Associate Professor in the Division of Forest Remote Sensing with SLU. In 2015, he also worked with the Vienna University of Technology, and in 2019, he was appointed as an Associate Professor with SLU. He has worked with various remote sensing methods, often focused on three-dimensional, including InSAR, radargrammetry, photogrammetry, and laser scanning. He participated in several EU and ESA projects, including Advanced SAR and GlobBiomass, and numerous local initiatives around the globe. He is the founder of Geoanalysis Sweden. Between 2009 and 2011, he worked in IT with ETH Zurich in Switzerland.

Lars M. H. Ulander (Fellow, IEEE) received the M.Sc. degree in engineering physics and the Ph.D. degree in electrical and computer engineering from the Chalmers University of Technology, Gothenburg, Sweden, in 1985 and 1991, respectively.

Since 2014, he has been a Professor in radar remote sensing with the Chalmers University of Technology. He also holds a part-time position with the Swedish Defence Research Agency (FOI), Linköping, where he is the Director of Research in radar signal processing and leads the research on very high frequency (VHF)/ultra high frequency (UHF)-band radar. He has authored or coauthored more than 300 professional publications, of which more than 80 are in peer-reviewed scientific journals. His research interests include radar imaging, SAR, signal processing, electromagnetic scattering models, and remote sensing applications.